miR-223-3p promotes microglial lactylation and M1 polarization via the FBXW7/Notch1/Hes1/SIRT1 axis

XIAOYU WANG[1*], LIN SONG[1-3*], JIAFENG WANG[1], QIANQIAN XIE[1], YAN WANG[1], CHUNYAN LI[1], TIANQI WANG[4] and YIFENG DU[1-3,5]

[1]Department of Neurology, Shandong Provincial Hospital Affiliated to Shandong First Medical University, Jinan, Shandong 250021, P.R. China; [2]Department of Neurology, Shandong Provincial Hospital, Shandong University, Jinan, Shandong 250021, P.R. China; [3]Shandong Provincial Clinical Research Center for Neurological Diseases, Jinan, Shandong 250021, P.R. China; [4]Department of Urology, Shandong Provincial Hospital Affiliated to Shandong First Medical University, Jinan, Shandong 250021, P.R. China; [5]Institute of Brain Science and Brain-Inspired Research, Shandong First Medical University and Shandong Academy of Medical Sciences, Jinan, Shandong 250117, P.R. China

Received November 26, 2025; Accepted April 22, 2026

DOI: 10.3892/ijmm.2026.5849

Abstract. Neuroinflammation is a hallmark of Alzheimer's disease (AD) and is closely linked to microglial M1 polarization. In the present study, miR-223-3p was identified as a critical regulator of microglial metabolic reprogramming. Analyses of Gene Expression Omnibus and AD Neuroimaging Initiative datasets revealed significant upregulation of miR-223-3p in the brain, blood, and cerebrospinal fluid of patients with AD. The overexpression of miR-223-3p promoted M1 polarization and increased reactive oxygen species (ROS) levels. Transcriptomic, metabolomic and Seahorse analyses revealed increased glycolysis, lactate production and lactylation, whereas inhibition of lactylation reduced M1 polarization and ROS accumulation. Mechanistically, miR-223-3p suppressed SIRT1 expression and directly targeted *FBXW7*, leading to activation of the Notch1/Hes1 pathway and further suppression of *SIRT1*. In summary, these findings demonstrate that miR-223-3p drives microglial lactylation-mediated M1 polarization through the FBXW7/Notch1/Hes1/SIRT1 signaling axis. The present study provides new insight into the role of lactylation in neuroinflammation and highlights miR-223-3p as a potential therapeutic target for AD.

Correspondence to: Professor Yifeng Du, Department of Neurology, Shandong Provincial Hospital Affiliated to Shandong First Medical University, 324 Jingwu Road, Jinan, Shandong 250021, P.R. China
E-mail: du-yifeng@hotmail.com

Dr Tianqi Wang, Department of Urology, Shandong Provincial Hospital Affiliated to Shandong First Medical University, 324 Jingwu Road, Jinan, Shandong 250021, P.R. China
E-mail: aurologyman@vip.qq.com

*Contributed equally

Key words: lactylation, microglial M1 polarization, Alzheimer's disease, microRNA-223-3p, SIRT1

Introduction

Alzheimer's disease (AD), the most common neurodegenerative disorder worldwide, imposes an increasing burden on aging societies (1). Beyond amyloid-β (Aβ) deposition and tau pathology, neuroimmune inflammation is now recognized as a central driver of disease progression (2,3). Activated microglia, particularly in the M1 proinflammatory state, exacerbate neuronal injury by releasing cytokines and reactive metabolites (4). Studies further indicate that the metabolic state of microglia is tightly coupled to their functional phenotypes (5). Nevertheless, the upstream molecular determinants connecting microglial polarization to metabolic dysregulation remain poorly defined.

Metabolic reprogramming, defined as the preferential utilization of glycolysis for energy production even under normoxic conditions, has recently attracted increasing attention because of its critical role in the pathogenesis of AD (6). Microglia undergo marked metabolic reprogramming during M1 polarization, leading to increased release of proinflammatory cytokines and metabolic byproducts, thereby contributing to AD progression (7). Lactylation, a newly recognized post-translational modification (PTM), is a direct consequence of metabolic reprogramming and plays a pivotal role in regulating microglial function (8,9). Lactylation facilitates the proinflammatory M1 phenotype and the secretion of associated cytokines in microglia while simultaneously exerting a positive feedback effect on glycolysis to further increase metabolic activity (9). Moreover, it has been previously reported elevated lactate levels and increased lactylation in the hippocampal microglia of both AD mouse models and patients (10). However, the upstream signaling pathways regulating microglial lactylation remain unclear.

Sirtuin 1 (SIRT1) belongs to the nicotinamide adenine dinucleotide (NAD^+)-dependent deacylase family and

represents one of the most extensively studied members of the sirtuin family (11,12). As a critical metabolic sensor, SIRT1 catalyzes the deacylation of a wide range of substrates and thereby regulates diverse biological processes, including cellular energy metabolism, genomic stability, inflammation and aging (13). In the central nervous system (CNS), SIRT1 is widely recognized as a key regulator of neuroinflammation, aging and metabolic signaling, and its impaired activity is associated with cognitive decline and neurodegeneration (12,14). Several lines of evidence have indicated that SIRT1 also exerts delactylase activity in the regulation of protein lactylation. In gastric cancer cells, overexpression of SIRT1 has been shown to reduce histone H3K18 lactylation levels (15). In the context of heart failure, SIRT1 attenuates the development of heart failure by reducing lactylation at lysine 1,897 of the α-myosin heavy chain protein (16). However, whether SIRT1 modulates lactylation in microglia and the mechanism through which its upstream regulatory pathways are organized remain unclear.

MicroRNAs (miRNAs or miRs), as potent posttranscriptional regulators, have been increasingly implicated in the modulation of neuroinflammation, energy metabolism and neurodegeneration (17). Among them, miR-223-3p has gained attention because of its established role in inflammatory signaling and immune cell activation, and studies have indicated that miR-223-3p expression is elevated in patients with AD (18,19). Moreover, several studies have demonstrated that miR-223-3p is also involved in the regulation of glucose metabolism. Intracellular miR-223-3p accumulation perturbs glucose and lipid metabolism in adipocyte models (20), and tumor glycolysis can be facilitated through a circABCB10/miR-223-3p/PFN2 axis (21). However, the precise mechanisms by which it contributes to microglial polarization and lactylation remain to be fully elucidated.

Therefore, in the present study, it was aimed to investigate the regulatory role of miR-223-3p in microglial polarization by performing molecular, metabolic, and functional assays. It was investigated how miR-223-3p modulates lactylation and microglial polarization to identify potential therapeutic targets for AD.

Materials and methods

RNA-seq data acquisition and processing. The miRNA expression profiles of patients with AD and cognitively normal controls were retrieved from the Gene Expression Omnibus (GEO) database (datasets: GSE16759 (parietal lobe tissues) (22) and GSE48552 (prefrontal cortex tissues) (23) https://www.ncbi.nlm.nih.gov/geo/). In addition, blood and cerebrospinal fluid (CSF) expression data were obtained from the GSE46579 (serum tissues) (24) and GSE212623 (25) datasets in the GEO and the Alzheimer's Disease Neuroimaging Initiative (ADNI) databases (https://adni.loni.usc.edu/). Differentially expressed miRNAs were identified using the 'limma' package in R software (version 4.2.1) (https://www.r-project.org/), applying thresholds of $P<0.05$ and |log2-fold change (log2FC)|>1. The resulting candidate miRNAs were retained for subsequent analyses.

Cell culture. The microglial cell line BV2 was purchased from American Type Culture Collection. BV2 microglia were cultured in Dulbecco's modified Eagle's medium (DMEM; high glucose; Gibco; Thermo Fisher Scientific, Inc.) supplemented with 10% fetal bovine serum (FBS; Gibco; Thermo Fisher Scientific, Inc.) and 1% penicillin-streptomycin solution (100 U/ml penicillin and 100 μg/ml streptomycin). The cells were maintained at 37˚C in a humidified atmosphere containing 5% CO_2.

Cell transfection. To modulate gene and miRNA expression, multiple transfection strategies have been employed. Synthetic miR-223-3p mimics and inhibitors were purchased from Shanghai GeneChem Co., Ltd. To upregulate miR-223-3p expression, $2x10^5$ cells were transfected with synthetic miR-223-3p mimics (final concentration: 50 nM), while a scrambled sequence served as the negative control (NC, 50 nM). Conversely, miR-223-3p inhibitors were applied to suppress endogenous expression (final concentration: 100 nM). To overexpress *SIRT1*, the Notch1 intracellular domain (NICD1) and *FBXW7*, full-length cDNAs were PCR-amplified and subcloned and inserted into the pcDNA3.1 backbone to construct the corresponding overexpression plasmids [oe-Ubiquitination (Ub), oe-SIRT1, oe-NICD1 and oe-FBXW7)], with the empty pcDNA3.1 vector used as the NC (oe-NC). All plasmids were purchased from GEBERAL BIOL company. BV2 or 293T cells were transfected with 2 μg plasmid DNA per well in 6-well plates, with the empty pcDNA3.1 vector used as the negative control (oe-NC). For RNA interference, small interfering RNA (siRNA) transfection targeting mouse Hes1 was purchased from GEBERAL BIOL company and transfected at a final concentration of 50 nM using Lipofectamine siRNA Transfection Reagent, and transfection efficiency was assessed by measuring protein levels 72 h post-transfection. All plasmid transfections were carried out using X-tremeGENE HP DNA Transfection Reagent (Roche Diagnostics) according to the manufacturer's protocol.

Liquid chromatography coupled with tandem mass spectrometry (LC-MS/MS) analysis. For metabolomic analysis of metabolites using LC-MS/MS, data were acquired in both positive and negative ion modes to ensure comprehensive coverage of the metabolic network. For metabolomic profiling, chromatographic separation was performed on a Shimadzu Nexera X2 LC-30AD ultrahigh-performance liquid chromatography (UHPLC) system equipped with an XBridge BEH C18 column. The column was maintained at 40˚C, with a mobile phase consisting of (A) water containing 5% acetonitrile and 10 mM ammonium acetate (pH 9.0) and (B) water containing 95% acetonitrile and 10 mM ammonium acetate (pH 9.0). The gradient program was set as follows: 0-2 min, 95% B; 2-9 min, linear decrease to 70% B; 9-10 min, further decrease to 30% B; 10-11 min, hold at 30% B; 11-11.5 min, return to 95% B; and 11.5-15 min, re-equilibration. The flow rate was 300 μl/min, the injection volume was 5 μl, and the autosampler was kept at 4˚C. Mass spectrometric detection was performed on a triple quadrupole linear ion trap system operated in multiple reaction monitoring (MRM) mode, with optimized parent-product ion transitions for targeted metabolites. The collision energy and declustering potential were adjusted on the basis of preliminary optimization. Data acquisition and processing were carried out using Analyst TF 1.7.1 software

(Shanghai AB SCIEX Analytical Instrument Trading Co.), with chromatographic peaks integrated via the Macleod algorithm and a minimum signal-to-noise ratio of 3:1 as the cutoff for detection. Intracellular lactate concentration was measured with a Lactate Content Assay kit (cat. no. AKAC001-1M-50S; Beijing Boxbio Science & Technology, Co., Ltd.), following the manufacturers' protocols.

Extracellular acidification rate (ECAR). The ECAR was assessed using the Seahorse XF Glycolysis Stress Test (Agilent Technologies, Inc.). Briefly, cells ($4x10^4$ per well) were seeded into XF24 microplates and cultured overnight. On the day of measurement, the cells were equilibrated in Seahorse assay medium, and the ECAR was monitored at baseline, followed by sequential injections of 10 mM glucose, 1 μM oligomycin (cat. no. HY-N6782; MedChemExpress) and 50 mM 2-deoxy-D-glucose (2-DG; cat. no. HY-13966; MedChemExpress). Basal glycolysis and glycolytic capacity were determined according to the manufacturer's protocol.

Oxygen consumption rate (OCR). For the OCR assessment, the culture medium was replaced 1 h prior to the assay with mitochondrial stress test buffer consisting of Seahorse XF Base Medium supplemented with 10 mM glucose, 2 mM glutamine and 1 mM pyruvate. The microplates were subsequently incubated at 37˚C in a CO_2-free chamber. In accordance with the manufacturer's instructions, an XF sensor cartridge sequentially delivered respiratory modulators to reach final concentrations of oligomycin (1.5 μM), FCCP (0.5 μM) and rotenone/antimycin A (0.5 μM).

Reverse transcription-quantitative PCR (RT-qPCR). Total RNA was isolated using SteadyPure Universal RNA Extraction Kit II (cat. no. AG21022; Hunan Accurate Bio-Medical Co., Ltd.), and complementary DNA was synthesized with Evo M-MLV RT Mix Kit with gDNA Clean for qPCR Ver. 2 (cat. no. AG1728; Hunan Accurate Bio-Medical Co., Ltd.) following the manufacturer's protocol. RT-qPCR was subsequently conducted with SYBR Green Premix Pro Taq HS qPCR Kit (cat. no. AG11701; Hunan Accurate Bio-Medical Co., Ltd.) on Light Cycler@480 System (Roche Diagnostics). The thermocycling conditions were as follows: Initial denaturation at 95˚C for 30 sec; followed by 40 cycles of denaturation at 95˚C for 5 sec and annealing/extension at 60˚C for 30 sec. β-actin was used as an internal control to standardize relative mRNA levels. miR-223-3p expression was quantified using stem-loop reverse transcription followed by qPCR. Briefly, a miRNA-specific stem-loop RT primer was used to selectively reverse transcribe mature miRNA, and RT-qPCR was performed using a miRNA-specific forward primer and a universal reverse primer. The U6 gene was used as an internal control. All PCR primers were designed and synthesized by GENERAL BIOL Biotech and are listed in Table SI.

Western blotting. For cellular lysate, cells were washed with 1X PBS and then lysed in RIPA buffer (cat. no. G2002; Wuhan Servicebio Technology Co., Ltd.) supplemented with Halt protease inhibitor (cat. no. G2008; Wuhan Servicebio Technology Co., Ltd.) for 20 min at 4˚C. The lysate was subsequently centrifuged at 14,000 x g for 5 min at 4˚C to pellet insoluble material. Protein concentrations in the extracts were determined using the bicinchoninic acid (BCA) assay (cat. no. P0012; Beyotime Institute of Biotechnology) against a bovine serum albumin standard curve. Protein samples (10 μl per lane) were loaded into Bolt 10-12% Tris-Glycine Plus gels and subsequently transferred onto polyvinylidene difluoride membranes. After blocking with an appropriate reagent, the membranes were incubated with the indicated primary antibodies overnight at 4˚C, followed by incubation with horseradish peroxidase-conjugated secondary antibodies for 1 h at room temperature. The membranes were rinsed three times with TBST (0.1% Tween, 10 min each), and protein signals were detected using an enhanced chemiluminescence (ECL) system (cat. no. KF8001; Affinity Biosciences). Detailed information on the primary and secondary antibodies employed is summarized in Table SII. The band intensities were quantified using ImageJ software (version 1.54g; National Institutes of Health) and normalized to the β-actin.

Co-immunoprecipitation (Co-IP) assay. 293T and BV2 cells were lysed in 500 μl of IP lysis buffer (cat. no. P70100; New Cell & Molecular Biotech) containing phenyl-methyl sulfonyl fluoride. The lysates were centrifuged at 12,000 x g for 10 min at 4˚C, and the clarified supernatants were incubated overnight at 4˚C with the indicated antibody and Protein A/G agarose beads (20 μl; cat. no. sc-2003; Santa Cruz Biotechnology, Inc.) under gentle rotation. After six washes with the designated buffer, the bound proteins were eluted and subjected to western blot analysis as aforementioned.

Functional enrichment analysis. The functional characterization of differentially expressed genes (DEGs) was conducted through Kyoto Encyclopedia of Genes and Genomes (KEGG) pathway enrichment analysis. KEGG enrichment was implemented using the R package clusterProfiler to identify biologically relevant signaling pathways (26). In addition, gene set enrichment analysis (GSEA) was performed with hallmark gene sets retrieved from the Molecular Signatures Database (MSigDB; http://www.gsea-msigdb.org/gsea/downloads.jsp) (27,28).

Receiver operating characteristic (ROC) analysis. ROC curve analysis was performed to evaluate the diagnostic performance of miR-223-3p in patients with AD. ROC curves were constructed by plotting sensitivity (true positive rate) against 1-specificity (false positive rate) across a range of cutoff values. The area under the ROC curve (AUC) was calculated as a quantitative measure of diagnostic accuracy. An AUC of 0.5 indicates no discriminative ability, whereas an AUC of 1.0 represents perfect diagnostic performance; therefore, values closer to 1 indicate improved diagnostic accuracy. Sensitivity, specificity, and the corresponding 95% confidence intervals (CIs) were calculated to further assess diagnostic reliability.

Reactive oxygen species (ROS) assay. BV2 microglia in the logarithmic growth phase were plated in six-well plates at a density of $3x10^5$ cells per well. For detection, cells were incubated with 5 μM C11-BODIPY (Thermo Fisher Scientific, Inc.) at 37˚C for 30 min, followed by washing and flow cytometric analysis using a Beckman Coulter CytoFLEX S (Beckman

Coulter, Inc.) according to the manufacturer's instructions. ROS levels were quantified in the FITC channel.

Drug treatment. To inhibit glycolytic activity, BV2 microglia were incubated for 24 h with oxamate (10 mM; cat. no. HY-W013032A; MedChemExpress) and 2-DG (10 mM; cat. no. HY-13966; MedChemExpress). The SIRT1 inhibitor EX527 (10 μM; 49843-98-3; TargetMol) and the SIRT1 activator SRT1720 (5 μM; 1001645-58-4; TargetMol) were added separately and incubated for 24 h. The γ-secretase inhibitor DAPT (20 nM; cat. no. HY-13027; MedChemExpress) was administered in parallel experiments, while DMSO served as the vehicle control.

Cell Counting Kit-8 (CCK-8) assay. To determine the half-maximal inhibitory concentration (IC_{50}) values, BV2 cells were seeded at 10,000 cells per well into 96-well plates and treated with increasing concentrations of oxamate or 2-DG for 24 h. The medium was then replaced, 10 μl of CCK-8 solution (Beijing LABLEAD, Inc.) was added to each well, and the absorbance at 450 nm was measured using a microplate reader (Multiskan FC; Thermo Fisher Scientific, Inc.). Cell viability was assessed according to the manufacturer's instructions, and the IC_{50} values were calculated based on dose-response curves.

Cycloheximide (CHX) chase assay. BV2 cells were plated in 12-well culture plates at a density of $3x10^5$ cells per well. After attachment, they were exposed to 2 μM CHX (66-81-9; TargetMol) for the designated time periods, followed by cell lysis and protein extraction for western blotting.

Ubiquitylation assay. 293T cells were transfected with Ub, Myc-FBXW7 and His-NICD1 expression plasmids for 48 h, followed by exposure to MG132 (10 μM; cat. no. 133407-82-6, TargetMol) for 4 h. After treatment, the cells were rinsed with PBS and lysed, and immunoprecipitation was performed using 20 μl of proteinA/G beads (cat. no. sc-2003; Santa Cruz Biotechnology, Inc.). The precipitated proteins were then subjected to western blotting, and Notch1 ubiquitination was detected with an anti-Ub antibody.

Dual-luciferase reporter assay. Complementary oligonucleotide pairs containing either the wild-type (WT) or the mutant (MUT) sequence of the *FBXW7* target region were designed and synthesized by Shanghai GenePharma Co., Ltd. The annealed fragments were subsequently cloned and inserted into the pmirGLO Dual-Luciferase miRNA Target Expression Vector (Promega Corporation). For the reporter assay, cells were seeded in 24-well plates and co-transfected with 100 ng of the FBXW7 reporter plasmid (WT or MUT) and 50 nM miR-223-3p mimics or negative control using Lipofectamine 3000 (Thermo Fisher Scientific, Inc.). A total of 48 h after transfection, luciferase activity was determined using a dual-luciferase assay system (cat. no. E1910; Promega Corporation) and normalized to *Renilla* luciferase activity.

Statistical analysis. Data distribution was first examined with normality tests. Comparisons between two groups with normally distributed variables were performed with unpaired t-tests, whereas one-way ANOVA was applied for analyses involving three groups, followed by Bonferroni's post hoc test to adjust for multiple comparisons. When the data deviated from normality, Wilcoxon rank-sum and Kruskal-Wallis tests were used for two- and three-group comparisons, respectively. The results are expressed as the mean ± standard deviation (SD), and all analyses were two-tailed, with statistically significant difference set at $P<0.05$. All the statistical analyses and data visualization were performed using GraphPad Prism (version 8.0; Dotmatics) and R software (version 4.2.1).

Results

miR-223-3p is dysregulated in patients with AD. miR-223-3p expression was significantly altered in patients with AD across multiple brain regions and biofluids. In the GEO datasets, miR-223-3p levels were significantly increased in the parietal lobe tissues of patients with AD compared with controls (GSE16759, P=0.032; Fig. 1A). A similar upregulation was observed in the prefrontal cortex (GSE48552, P=0.002; Fig. 1B). Consistently, peripheral samples also showed elevated miR-223-3p levels in AD. In the GEO dataset GSE46579, both serum and CSF from patients with AD exhibited significantly higher miR-223-3p levels than those from controls (both $P<0.001$; Fig. 1C and D). These findings were further validated using the ADNI cohort. Compared with controls, patients with AD demonstrated significantly increased miR-223-3p levels in both serum and CSF samples ($P<0.001$ for both comparisons; Fig. 1E and F), confirming the consistent dysregulation of miR-223-3p across independent datasets and sample types.

To evaluate the diagnostic performance of miR-223-3p for AD, ROC curve analyses were performed. In brain tissues from the GEO dataset, miR-223-3p showed excellent discriminative ability, with an AUC of 0.938 (95% CI: 0.764-1.000) in the parietal lobe (Fig. 1G) and 0.972 (95% CI: 0.895-1.000) in the prefrontal cortex (Fig. 1H). In peripheral samples, the AUC was 0.820 (95% CI: 0.705-0.935) for serum (Fig. 1I) and 0.943 (95% CI: 0.879-1.000) for CSF in the GEO dataset (Fig. 1J). Similar diagnostic performance was observed in the ADNI cohort, with AUC values of 0.860 (95% CI: 0.797-0.924) for serum (Fig. 1K) and 0.825 (95% CI: 0.758-0.892) for CSF (Fig. 1L). Taken together, these results indicate that miR-223-3p is consistently upregulated in both brain tissues and biofluids of AD patients and exhibits promising diagnostic value for distinguishing AD from controls.

miR-223-3p promotes microglial M1 polarization. To explore the role of miR-223-3p in microglial functions, *in vitro* microglial polarization experiments were designed. BV2 microglia were used to establish three experimental conditions: NC, miR-223-3p mimic and miR-223-3p inhibitor. RT-qPCR verified the efficient modulation of miR-223-3p expression among the groups (Fig. 2A). Functionally, miR-223-3p overexpression increased the transcription of M1-associated markers [iNOS (inducible nitric oxide synthase), IL-1β and TNF-α] but suppressed M2-associated markers (Arg-1, YM-1 and FIZZ1) (Fig. 2B). Western blotting further demonstrated elevated iNOS protein levels and reduced Arg-1 levels in miR-223-3p-overexpressing cells (Fig. 2C). In addition, flow cytometry revealed a pronounced increase in ROS levels following miR-223-3p overexpression (Fig. 2D). Collectively, these findings suggest

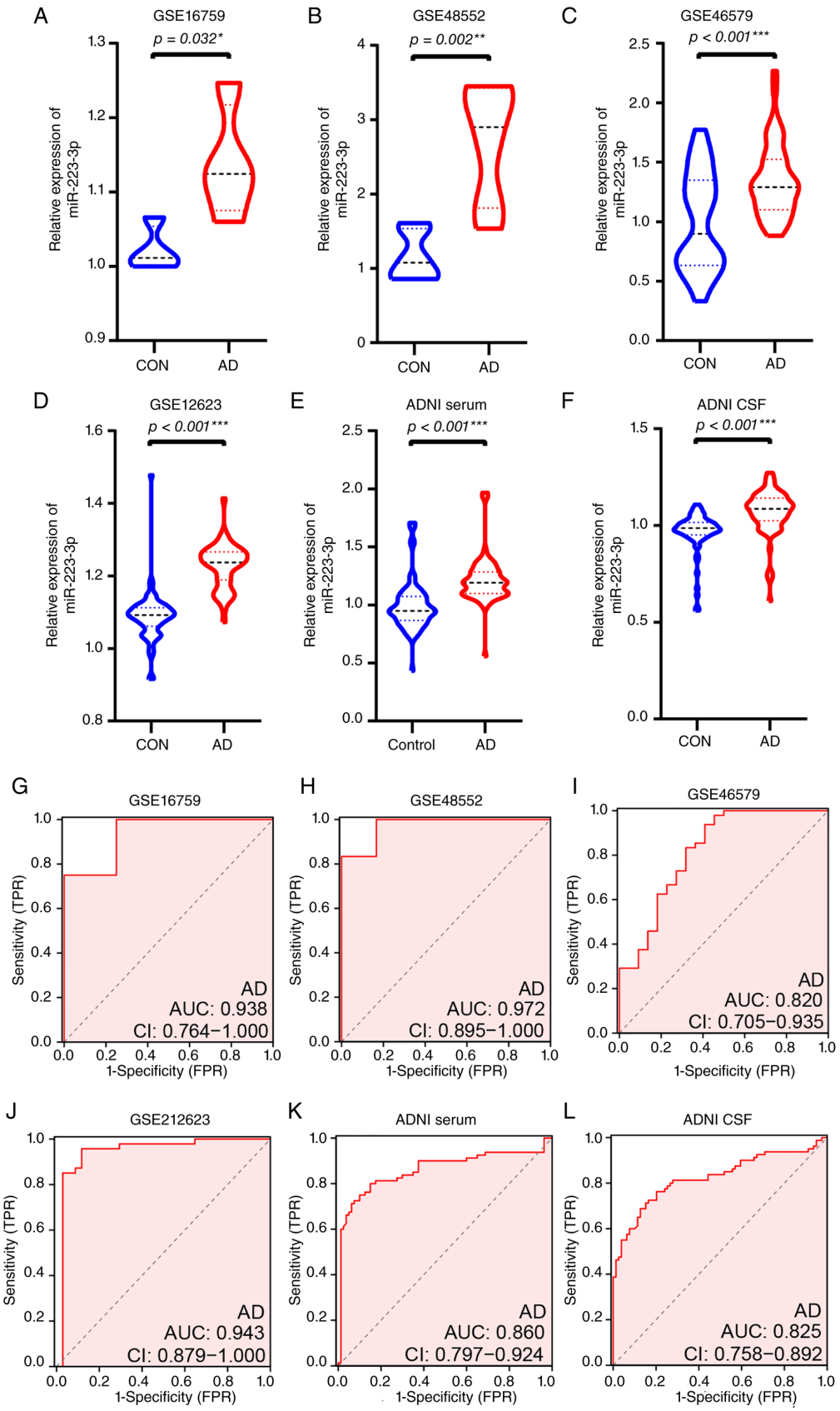

Figure 1. miR-223-3p is dysregulated in patients with AD. (A and B) Expression of miR-223-3p in (A) parietal lobe tissues and (B) prefrontal cortex tissues of patients with AD compared with controls. (C and D) miR-223-3p levels in both (C) serum and (D) CSF samples from patients with AD relative to those from controls in the GEO dataset. (E and F) miR-223-3p levels in both (E) serum and (F) CSF samples from patients with AD relative to those from controls according to the ADNI dataset. (G) ROC curve of miR-223-3p in parietal lobe tissues for AD from GEO dataset. (H) ROC curve of miR-223-3p in prefrontal cortex tissues for AD from GEO dataset. (I) ROC curves of miR-223-3p in serum for AD from GEO dataset. (J) ROC curves of miR-223-3p in CSF for AD from GEO dataset. (K) ROC curves of miR-223-3p in serum for AD from ADNI dataset. (L) ROC curves of miR-223-3p in CSF for AD from ADNI dataset. *P<0.05, **P<0.01 and ***P<0.001. miR, microRNA; AD, Alzheimer's disease; CSF, cerebrospinal fluid; GEO, Gene Expression Omnibus; ADNI, AD Neuroimaging Initiative; ROC, receiver operating characteristic; AUC, area under the curve; CI, confidence interval.

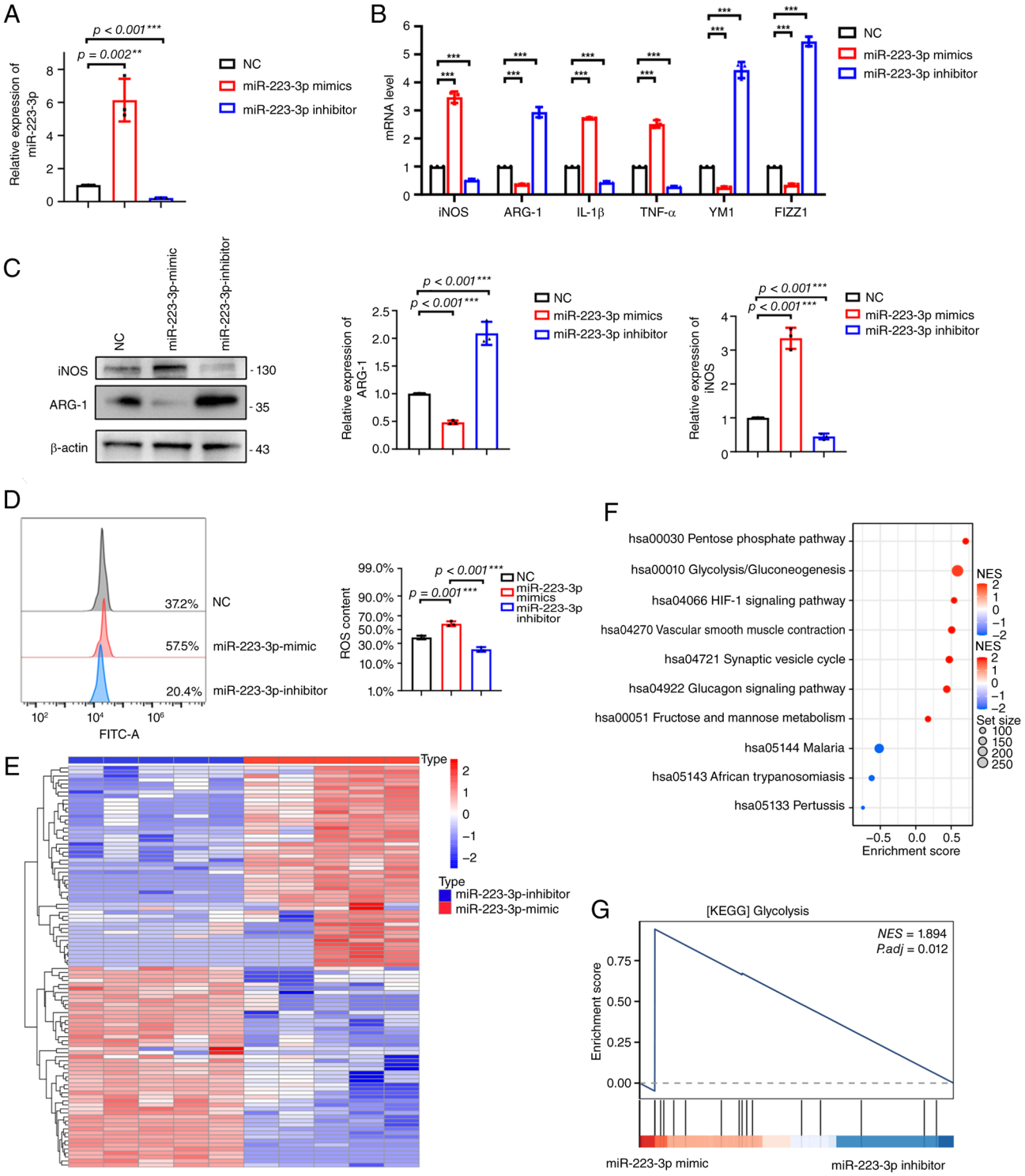

Figure 2. miR-223-3p promotes microglial M1 polarization. (A) RT-qPCR analysis of miR-223-3p expression. (B) RT-qPCR analysis of M1/M2 polarization marker genes in microglia. (C) Western blot detection of iNOS and Arg-1 protein levels. (D) Flow cytometric analysis of ROS levels. (E) Heatmap of genes differentially expressed between the high- and low-miR-223-3p groups. (F) KEGG pathway enrichment analysis of differentially expressed genes. (G) Gene Set Enrichment Analysis of glycolysis-associated pathways in miR-223-3p-regulated microglia. **P<0.01 and ***P<0.001. miR, microRNA; RT-qPCR, reverse transcription-quantitative PCR; iNOS, inducible nitric oxide synthase; ROS, reactive oxygen species; KEGG, Kyoto Encyclopedia of Genes and Genomes; NC, negative control.

that miR-223-3p drives microglial polarization toward the proinflammatory M1 phenotype.

To elucidate the molecular basis of this phenotype, two groups of microglia were subjected to transcriptome sequencing (Fig. 2E). KEGG pathway enrichment revealed that glycolysis/gluconeogenesis and HIF-1 signaling were significantly altered (Fig. 2F). GSEA further confirmed the enrichment of glycolysis in the miR-223-3p mimic group (Fig. 2G). These results illustrated that the M1 proinflammatory phenotype may be associated with increased aerobic glycolysis.

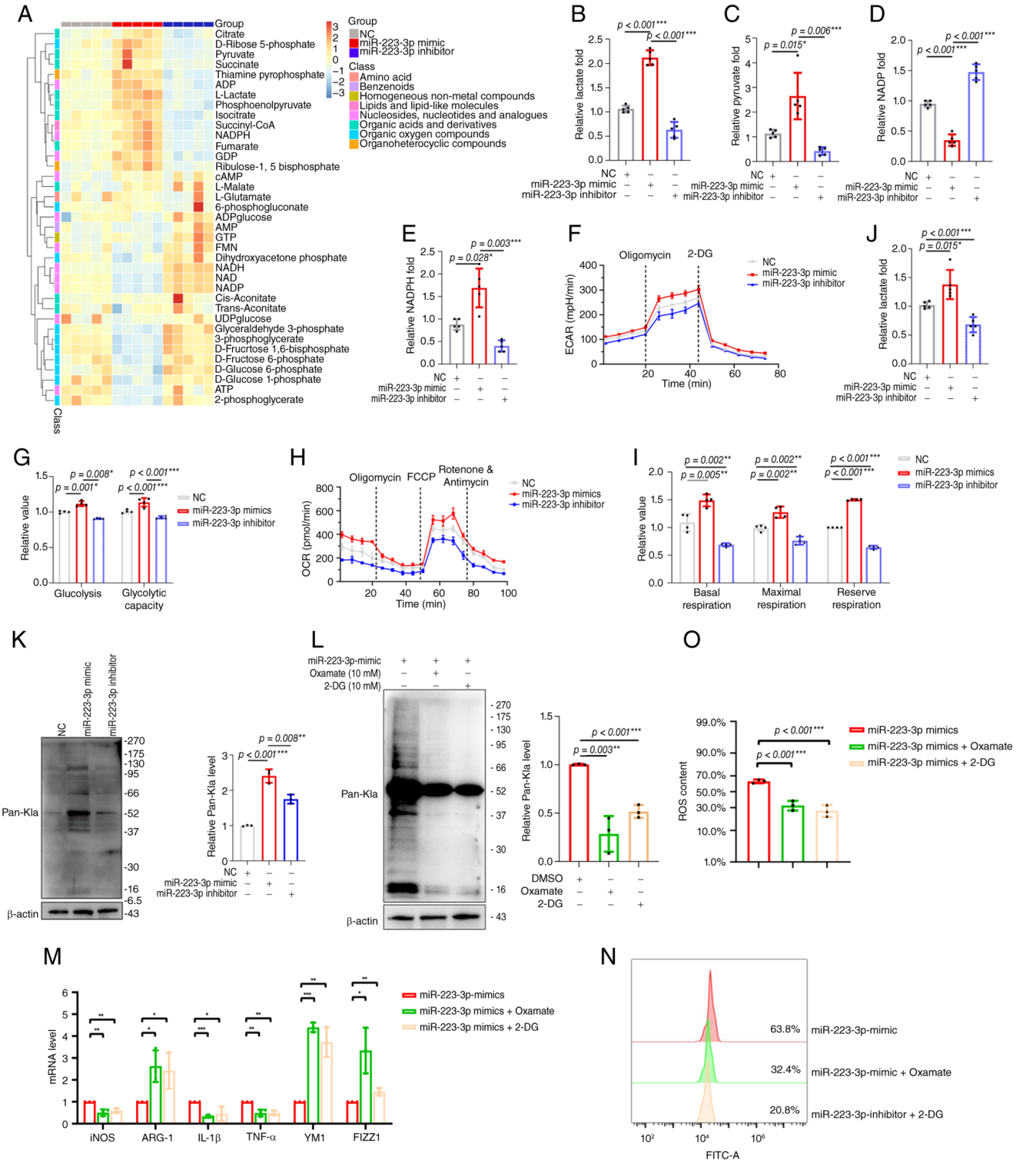

Figure 3. miR-223-3p promotes microglial M1 polarization through the regulation of lactylation. (A) Heatmap of metabolite profiles across three experimental groups. (B-E) LC-MS/MS quantification of (B) lactate, (C) pyruvate, (D) $NADP^+$ and (E) NADPH levels. (F and G) ECAR assays measuring basal and compensatory glycolysis. (H and I) OCR assays assessing mitochondrial respiration. (J) Lactate content assay assessing intracellular lactate level. (K) Western blot analysis of global lactylation levels. (L) Western blot analysis of lactylation levels following treatment with glycolytic inhibitors oxamate (10 mM; 24 h) and 2-DG (10 mM; 24 h). (M) Reverse transcription-quantitative PCR analysis of microglial polarization markers. (N and O) Flow cytometric analysis of ROS levels. *P<0.05, **P<0.01 and ***P<0.001. miR, microRNA; ECAR, extracellular acidification rate; OCR, oxygen consumption rate; 2-DG, 2-deoxy-D-glucose; ROS, reactive oxygen species; NC, negative control.

miR-223-3p promotes microglial M1 polarization through glycolysis-linked lysine lactylation. To assess whether miR-223-3p reshapes microglial glucose metabolism, LC-MS/MS-based metabolomics were performed on BV2 cells transduced with NC, a miR-223-3p mimic, or a miR-223-3p inhibitor. A heatmap revealed robust, group-dependent shifts in metabolite profiles (Fig. 3A). Targeted quantification revealed that miR-223-3p overexpression increased the levels

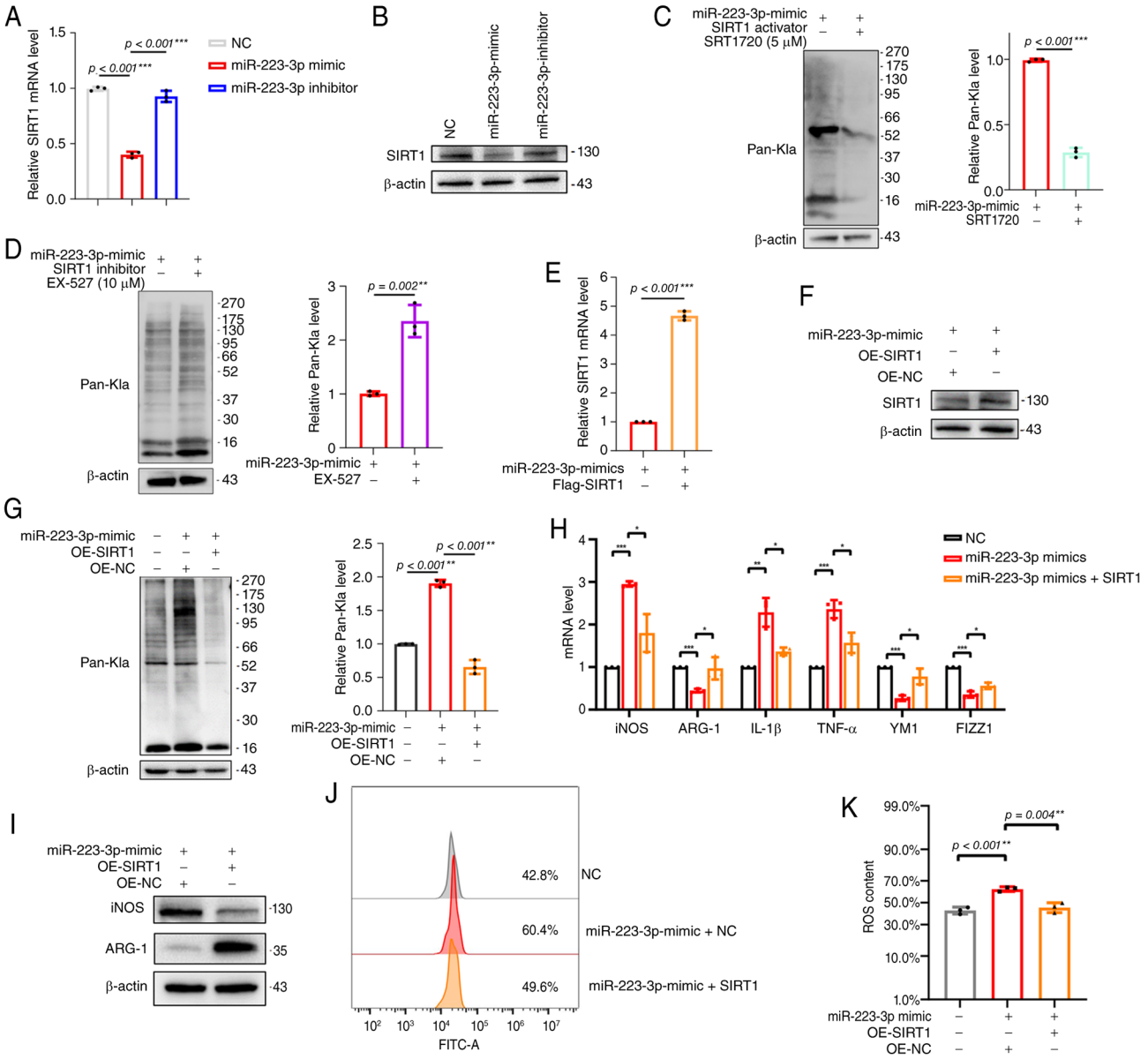

Figure 4. miR-223-3p promotes microglial lactylation and M1 polarization by suppressing SIRT1 expression. (A) RT-qPCR analysis of *SIRT1* mRNA expression. (B) Western blot analysis of SIRT1 protein levels. (C) Western blot analysis of lactylation levels following treatment with SIRT1 activator SRT1720 (5 μM; 24 h). (D) Western blot analysis of lactylation levels following treatment with SIRT1 inhibitor EX-527 (10 μM; 24 h). (E and F) RT-qPCR and Western blot validation of SIRT1 overexpression in rescue experiments. (G) Western blot detection of global lactylation levels. (H) RT-qPCR analysis of microglial polarization markers. (I) Western blot analysis of iNOS and Arg-1 protein expression. (J and K) Flow cytometric analysis of ROS levels. *P<0.05, **P<0.01 and ***P<0.001. miR, microRNA; SIRT1, sirtuin 1; RT-qPCR, reverse transcription-quantitative PCR; iNOS, inducible nitric oxide synthase; ROS, reactive oxygen species; NC, negative control; OE, overexpression.

of lactate (Fig. 3B) and pyruvate (Fig. 3C), reduced the level of $NADP^+$ (Fig. 3D), and increased the level of NADPH (Fig. 3E). Seahorse assays further demonstrated that miR-223-3p increased the ECAR, increasing both basal and compensatory glycolysis (Fig. 3F and G), and increased the OCR, increasing basal, maximal and spare respiratory capacity (Fig. 3H and I). Consistent with the metabolomics data, lactate content was greater in the miR-223-3p mimic group (Fig. 3J). Western blotting confirmed a concomitant increase in global protein lactylation (Fig. 3K).

To evaluate the potential cytotoxic effects of glycolytic inhibition, BV2 cells were treated with increasing concentrations of oxamate or 2-DG, and cell viability was assessed using a CCK-8 assay. The calculated IC_{50} values were 31.70 mM for oxamate and 26.56 mM for 2-DG (Fig. S1A and B). Based on these results, 10 mM oxamate and 10 mM 2-DG, which are well below their respective IC_{50} values, were selected for subsequent experiments to suppress lactylation (Fig. 3L). Inhibiting protein lactylation attenuated the miR-223-3p-induced transcription of M1 markers (iNOS, IL-1β and TNF-α) while restoring the expression of M2 markers (Arg-1, YM-1 and FIZZ1) (Fig. 3M). Lactylation inhibition also reduced intracellular ROS levels (Fig. 3N and O). These results indicate that miR-223-3p promotes microglial M1 polarization through glycolysis-associated lysine lactylation.

miR-223-3p enhances microglial lactylation via SIRT1 suppression, ultimately contributing to M1 polarization.

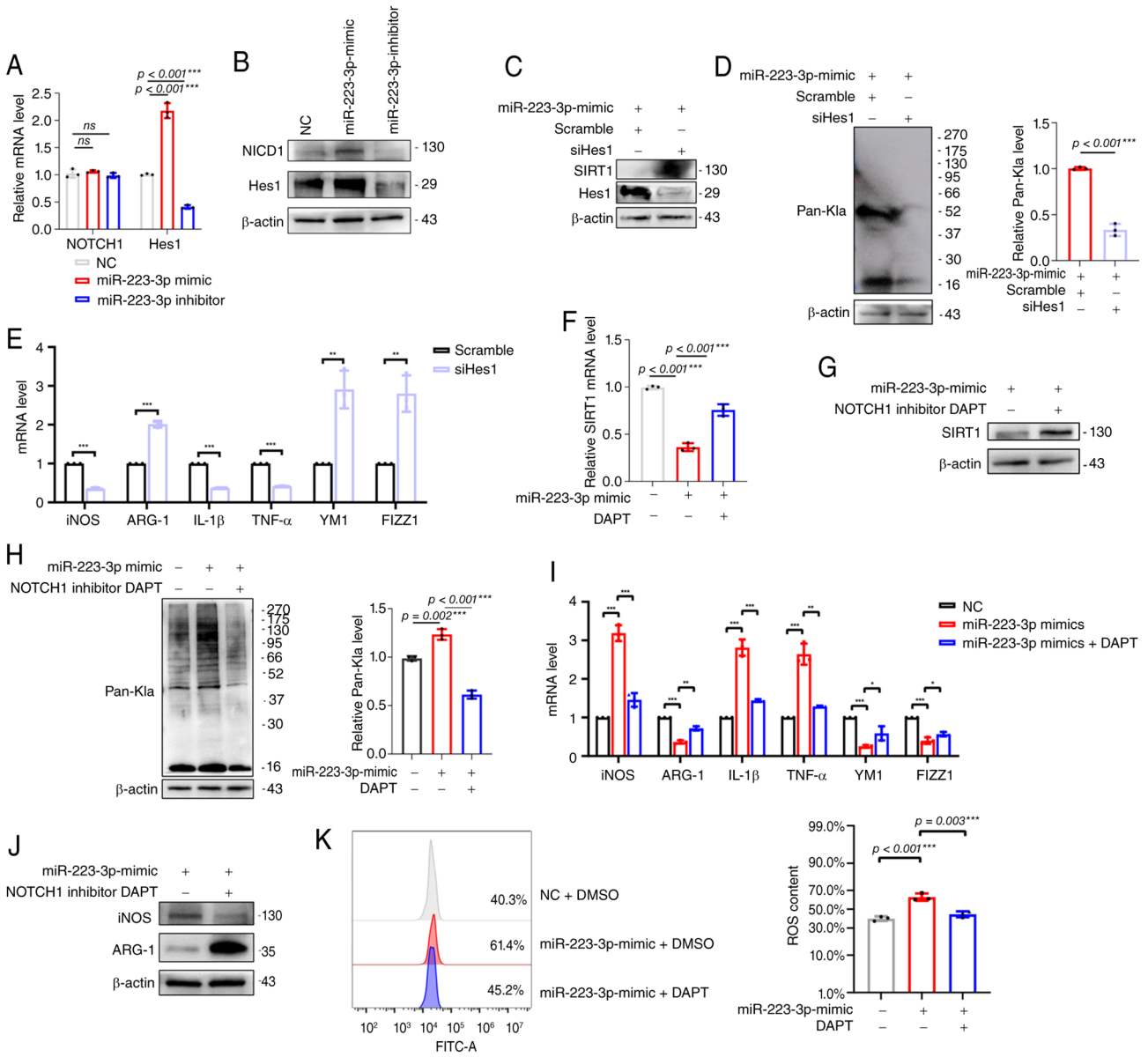

Figure 5. miR-223-3p suppresses SIRT1 transcription via the Notch1/Hes1 signaling pathway, thereby promoting microglial lactylation and M1 polarization. (A) RT-qPCR analysis of *Notch1* and *Hes1* mRNA levels. (B) Western blot analysis of NICD1 and Hes1 protein expression. (C) Western blot analysis of SIRT1 expression following silencing Hes1. (D) Western blot detection of global lactylation levels. (E) RT-qPCR analysis of microglial polarization markers. (F and G) RT-qPCR and western blot detection of SIRT1 following treatment with Notch1 inhibitor DAPT (20 nM; 24 h). (H) Western blot detection of global lactylation levels. (I) RT-qPCR analysis of microglial polarization markers. (J) Western blot analysis of iNOS and Arg-1 protein expression. (K) Flow cytometric analysis of ROS levels. *P<0.05, **P<0.01 and ***P<0.001. miR, microRNA; SIRT1, sirtuin 1; RT-qPCR, reverse transcription-quantitative PCR; iNOS, inducible nitric oxide synthase; ROS, reactive oxygen species; NC, negative control; ns, not significant.

SIRT1 is a known delactylase that regulates protein lactylation. RT-qPCR and western blotting revealed that miR-223-3p suppressed both the transcription and translation of *SIRT1* (Fig. 4A and B). To explore the potential mechanism underlying miR-223-3p-mediated regulation of lactylation, it was examined whether SIRT1 influences protein lactylation levels. The western blot results showed that treatment with the SIRT1 activator SRT1720 significantly decreased the overall Pan-Kla signal compared with the control group (Fig. 4C). By contrast, inhibition of SIRT1 with EX-527 resulted in a clear increase in Pan-Kla levels (Fig. 4D). To confirm causality, SIRT1 was reintroduced into wild-type and miR-223-3p mimic-transfected BV2 cells (Fig. S2A; Fig. 4E and F). Western blotting revealed that SIRT1 overexpression attenuated the increase in lactylation induced by miR-223-3p (Fig. 4G). Consistently, both RT-qPCR and western blotting demonstrated that restoring SIRT1 expression reduced the expression of M1 polarization markers (iNOS, IL-1β and TNF-α) (Fig. 4H and I). Furthermore, while miR-223-3p elevated ROS levels in microglia, SIRT1 overexpression diminished ROS accumulation (Fig. 4J and K).

miR-223-3p promotes microglial lactylation and M1 polarization by repressing SIRT1 transcription through the Notch1/Hes1 signaling pathway. The Notch1/Hes1 signaling axis has been reported to repress SIRT1 transcription by directly binding to its promoter (29). However, whether miR-223-3p utilizes this pathway to regulate SIRT1 remains unclear. The present RT-qPCR analysis revealed that miR-223-3p

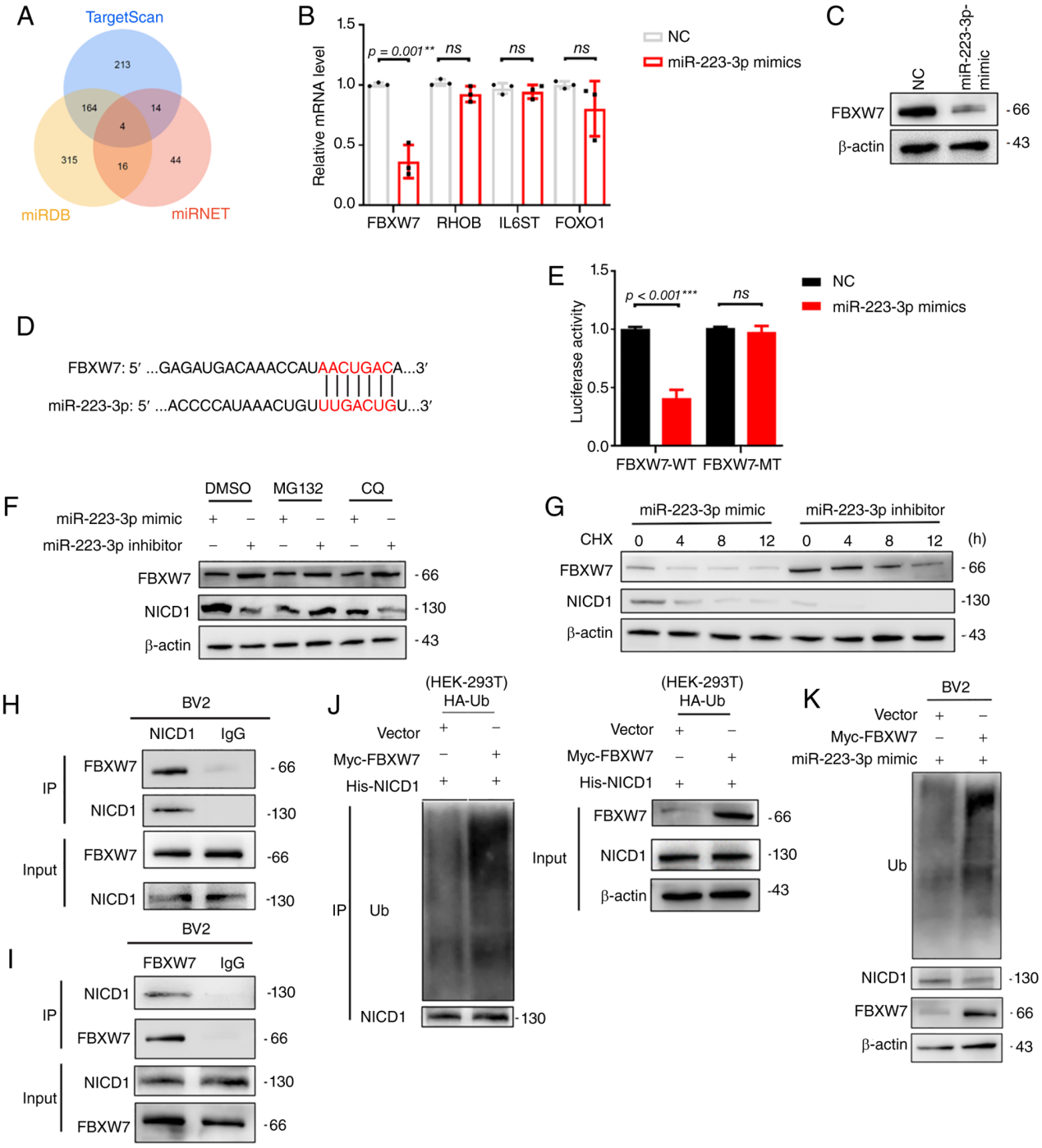

Figure 6. miR-223-3p targets FBXW7 to reduce Notch1 ubiquitination and degradation. (A) Venn diagram showing the overlap of predicted miR-223-3p targets from three databases. (B) Reverse transcription-quantitative PCR analysis of downstream target mRNA expression. (C) Western blot detection of FBXW7 protein expression. (D) Predicted binding site between miR-223-3p and the 3' untranslated region of *FBXW7*. (E) Dual-luciferase reporter assay confirming the direct interaction between miR-223-3p and *FBXW7*. (F) Effects of the proteasome inhibitor MG132 and the lysosomal inhibitor CQ on NICD1 protein expression in BV2 cells with altered miR-223-3p expression. (G) CHX chase assay showing the dynamics of NICD1 protein degradation in BV2 cells. (H and I) Co-immunoprecipitation analysis of the interaction between FBXW7 and NICD1. (J) Effect of FBXW7 overexpression on NICD1 ubiquitination in 293T cells. (K) Western blot analysis of FBXW7-mediated regulation of NICD1 expression and ubiquitination in microglia. **P<0.01 and ***P<0.001. miR, microRNA; CHX, cycloheximide; NC, negative control; ns, not significant.

significantly upregulated *Hes1* mRNA levels but had no effect on *Notch1* transcription (Fig. 5A). However, western blotting revealed that miR-223-3p increased the protein expression of both Hes1 and NICD1 (Fig. 5B), suggesting that miR-223-3p may promote NICD1 protein stability or translation through indirect mechanisms. To further investigate the role of Hes1 in regulating microglial lactylation and inflammatory activation, siRNA-mediated knockdown of *Hes1* was performed in BV2 cells. Western blot analysis confirmed that Hes1 silencing significantly increased *SIRT1* expression compared with the control group (Fig. 5C). Consistently, the global level of Pan-Kla was significantly reduced following Hes1 knockdown (Fig. 5D). In addition, the expression of M1-associated inflammatory markers was significantly decreased (Fig. 5E).

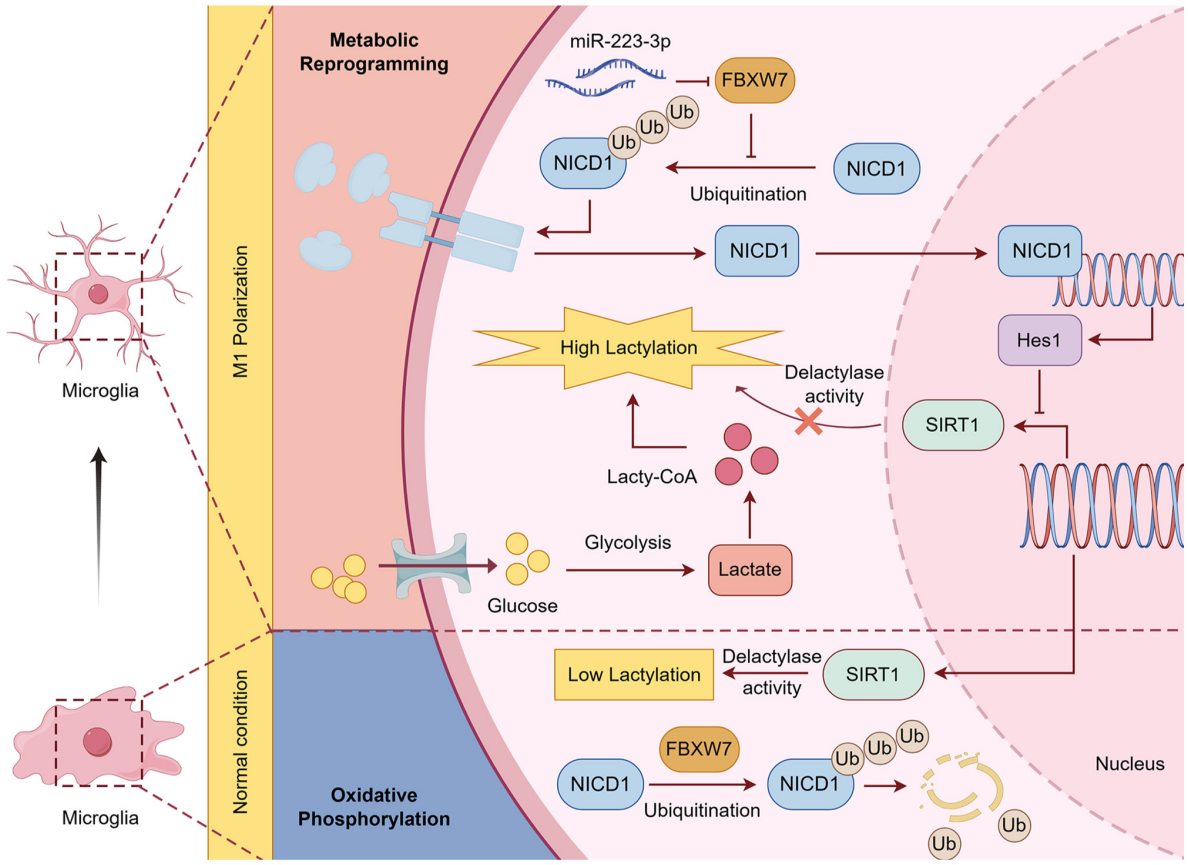

Figure 7. Schematic representation of the proposed mechanism of miR-223-3p in microglial M1 polarization. miR, microRNA; SIRT1, sirtuin 1.

To test functional involvement, the Notch1 inhibitor DAPT was applied. It was found that Notch1 inhibition also restored SIRT1 expression at both the transcript and protein levels (Fig. 5F and G). The inhibition of Notch1 attenuated the ability of miR-223-3p to increase lactylation (Fig. 5H) and drive microglial M1 polarization (Fig. 5I and J). Flow cytometry further confirmed that blocking Notch1 reduced the increase in ROS levels induced by miR-223-3p (Fig. 5K). These findings indicate that miR-223-3p activates the Notch1/Hes1 pathway to suppress *SIRT1* transcription, thereby promoting lactylation and skewing microglia toward the proinflammatory M1 phenotype.

miR-223-3p reduces NICD1 ubiquitination and degradation by targeting FBXW7. To elucidate how miR-223-3p regulates the Notch1/Hes1 signaling pathway, target prediction databases were first used and *FBXW7* was identified as a potential downstream target of miR-223-3p (Fig. 6A). RT-qPCR and western blot analyses confirmed that miR-223-3p suppressed *FBXW7* expression in microglia (Fig. 6B and C). The predicted binding site of miR-223-3p within the *FBXW7* 3' untranslated region is shown in Fig. 6D, and a dual-luciferase reporter assay confirmed the direct binding of miR-223-3p to *FBXW7* (Fig. 6E).

Next, it was explored whether miR-223-3p affects NICD1 degradation pathways. When proteasomal degradation was blocked, inhibition of miR-223-3p modestly increased NICD1 levels, whereas blocking lysosomal degradation reduced NICD1 expression (Fig. 6F). These results suggested that miR-223-3p promotes proteasome-dependent degradation of NICD1 via FBXW7 while stabilizing NICD1. Indeed, inhibiting miR-223-3p increased *FBXW7* expression, increased NICD1 degradation, and accelerated NICD1 turnover following CHX treatment (Fig. 6G). Interactions between FBXW7 and NICD1 were verified by co-IP assays (Fig. 6H and I). Moreover, FBXW7 overexpression promoted the ubiquitination and degradation of NICD1 in both 293T and BV2 cells (Fig. S2B-D; Fig. 6J and K). These findings demonstrate that miR-223-3p directly targets and represses *FBXW7*, thereby reducing NICD1 ubiquitination and proteasomal degradation, which stabilizes NICD1 and facilitates downstream Notch1/Hes1 signaling.

Discussion

In the present study, the results of transcriptomic analyses indicated that the expression of miR-223-3p was upregulated in the brain tissue, blood and CSF of individuals with AD and exhibited potential diagnostic value. The results of functional assays, including the assessment of microglial polarization markers, metabolomic profiling and metabolic flux measurements, suggested that miR-223-3p facilitates M1 microglial polarization through the increase in protein lactylation. Mechanistic investigations and rescue experiments further demonstrated that miR-223-3p suppressed FBXW7 expression, thereby attenuating the ubiquitin-proteasome-mediated degradation of NICD1. The stabilization of NICD1 consequently activated the Notch1/Hes1 signaling cascade, leading to reduced SIRT1 transcription and increased lactylation (Fig. 7).

Neuroimmune inflammation is considered a central mechanism in the pathogenesis of AD and is characterized by heightened immune cell activation and elevated levels of proinflammatory mediators (30). It has been shown that M1-polarized microglia further exacerbate neuronal injury through the release of inflammatory cytokines, thereby facilitating AD progression (31). Moreover, accumulating evidence has indicated that the metabolic states of microglia under different activation conditions are closely associated with their functional phenotypes (5). Similarly, in the present study, inhibition of glycolysis led to a reduction in the expression of M1 polarization markers in microglia, further supporting the notion that the metabolic state is critically associated with their phenotypic functions.

Lactylation was recently identified as a novel form of PTM in which lactate, a key metabolite of glycolysis, served as the substrate to directly regulate cellular metabolism, function and signaling pathways (8). Glycolysis, as a central pathway of energy metabolism, plays a critical role in microglial activation and functional regulation (32). When exposed to pathological stimuli such as Aβ deposition, trauma, or infection, microglia undergo pronounced metabolic reprogramming, shifting their metabolic profile from oxidative phosphorylation to aerobic glycolysis (33,34). This metabolic shift was particularly prominent in proinflammatory microglia (33). In the present study, a concurrent increase was observed in ECAR and OCR following miR-223-3p overexpression, suggesting that miR-223-3p enhances overall metabolic activity in microglia. This metabolic state may promote glycolysis-driven lactate production and protein lactylation while maintaining mitochondrial respiration to meet the increased energetic demands during inflammatory activation. Meanwhile, it was observed that miR-223-3p promoted M1 microglial polarization, which was accompanied by increased lactylation. The inhibition of microglial lactylation by glycolysis inhibitors, including oxamate and 2-DG, also suppressed M1 polarization. These findings suggest that lactylation may represent an important mechanism through which miR-223-3p drives microglial M1 polarization.

SIRT1, an NAD^+-dependent deacetylase, plays pivotal roles in energy metabolism, transcriptional regulation and cellular homeostasis and is regarded as an important modulator of cognitive function and the progression of neurodegenerative disorders (35,36). Experimental studies have demonstrated that activation of the NAD^+/SIRT1 pathway in AD animal models alleviated Aβ burden and improved cognitive impairment (37,38). Conversely, deletion of the SIRT1 gene markedly reduced neuronal mitochondrial biogenesis, leading to insufficient energy supply and excessive Aβ deposition, thereby accelerating AD pathology (39). Previous research further indicated that SIRT1 exerted anti-inflammatory effects in microglia, where increased activity suppressed the release of proinflammatory cytokines and promoted the maintenance of an anti-inflammatory phenotype (40). The present findings suggest that the protein lactylation observed in the present study is dependent on SIRT1 enzymatic activity. Reduced SIRT1 expression may limit its delactylase function, leading to the accumulation of lactylation and enhanced inflammatory gene expression.

The Notch1/Hes1 signaling pathway is a highly conserved intercellular communication mechanism that plays important roles in regulating cell proliferation, differentiation and metabolism. Recent studies have demonstrated that Notch1 signaling is closely linked to glycolysis. Specifically, NICD1 is localized to the mitochondrial matrix and directly activates pyruvate dehydrogenase, thereby promoting glycolysis in cardiac endothelial cells (41). Hes1, a classical downstream target of Notch1 signaling, functions as a transcriptional repressor by binding to gene promoters and suppressing transcriptional activity. Evidence has indicated that the Notch1/Hes1 axis markedly enhances aerobic glycolysis and promotes tumor progression in colorectal cancer cells (42). Notably, the role of Notch1 in the CNS has received increasing attention. It has been suggested that Notch1 modulates microglial cytokine secretion, phenotypic transformation and metabolic states, thereby contributing to the maintenance of brain homeostasis and the regulation of neuroinflammation (43). In the present study, it was observed that miR-223-3p activated the Notch1/Hes1 pathway, which significantly suppressed *SIRT1* expression. Treatment with the Notch1 inhibitor DAPT restored SIRT1 levels, further supporting the central role of the Notch1/Hes1 axis in regulating SIRT1 expression and the downstream process of protein lactylation. Consistently, silencing Hes1 also restored SIRT1 expression, indicating that Hes1 acts as a key transcriptional repressor of SIRT1 in this pathway.

The activity of the Notch1 receptor is tightly regulated by the ubiquitin-proteasome system (44). It has been demonstrated that the E3 ubiquitin ligase FBXW7 plays a critical role in the ubiquitination and degradation of Notch1. Specifically, FBXW7 recognized phosphorylated motifs within NICD1 and promoted its ubiquitin-mediated degradation, thereby negatively regulating the activity of the Notch1 signaling pathway (45). These findings indicated that FBXW7 functioned as an essential suppressor of the maintenance of Notch1 protein homeostasis. Consistent with earlier findings, the present study revealed that miR-223-3p targeted and suppressed FBXW7 expression, which attenuated Notch1 ubiquitination and degradation, leading to increased Notch1 protein stability and increased Notch1/Hes1 signaling activity. In line with previous studies that highlighted the significance of the interaction of miR-223-3p and *FBXW7* in various inflammatory and tumor models (46,47), the current results further revealed the critical role of this regulatory pathway in microglial lactylation and M1 polarization.

The present study revealed that miR-223-3p activated microglial lactylation and M1 polarization by targeting the FBXW7/Notch1/Hes1/SIRT1 signaling axis. These findings were consistent with previous evidence showing that aerobic glycolysis was markedly enhanced in M1-polarized microglia. Nevertheless, several limitations should be acknowledged. First, the experiments relied on the BV2 microglial cell line, which differs from primary human microglia and therefore might not fully reflect the *in vivo* state. Although BV2 cells serve as a well-established *in vitro* model for determining microglial signaling mechanisms, immortalized microglial lines may not fully reflect the physiological state of primary microglia in the brain microenvironment. Future studies using primary microglia and *in vivo* AD models will be needed to further validate the role of the miR-223-3p/FBXW7/Notch1/Hes1/SIRT1 regulatory axis identified in this study. Second, although the current findings suggested that miR-223-3p regulated

microglial lactylation via the FBXW7/Notch1/Hes1/SIRT1 axis, the underlying mechanisms require further validation in animal models to establish their physiological relevance. Further validation in animal models and mechanistic experiments will be needed to confirm causality. Third, the present study did not investigate the broader neuroinflammatory network or potential crosstalk between miR-223-3p and other metabolic or signaling pathways that may also contribute to AD progression. Future research should employ integrative approaches, such as multi-omics and systems biology analyses, to provide a more comprehensive understanding.

In conclusion, the present study revealed that miR-223-3p promoted microglial lactylation-mediated M1 polarization through the FBXW7/Notch1/Hes1/SIRT1 signaling axis. These findings expand the current understanding of lactylation in neuroinflammation and provide new insights into the interplay between microglial metabolism and inflammatory responses. Moreover, miR-223-3p may represent a potential therapeutic target for AD.

Acknowledgements

Not applicable.

Funding

The present study was supported by the STI2030-Major Project (grant nos. 2021ZD0201808 and 2022ZD0211600), the Academic Promotion Program of Shandong First Medical University (grant nos. 2019QL020 and 2020RC009), the Natural Science Foundation of Shandong (grant no. ZR2024MH225) and the Taishan Scholar Program of Shandong (grant nos. ts20190977 and Tsqn201909182).

Availability of data and materials

The data generated in the present study may be requested from the corresponding author.

Authors' contributions

XYW conceptualized the study, conducted formal analysis, investigation, data curation, statistical analysis and data visualization, provided resources and wrote the original draft of the manuscript. LS conceptualized and supervised the study, performed data visualization, and wrote, reviewed, and edited the manuscript. JFW and QQX conducted formal analysis, investigation and statistical analysis, and wrote, reviewed and edited the manuscript. YW and CYL conducted investigation and data visualization and reviewed and edited the manuscript. TQW and YFD conceptualized and supervised the study, performed data visualization, and wrote, reviewed and edited the manuscript. All the authors had access to and verified the data used in the present study. All authors read and approved the final version of the manuscript and confirm the authenticity of all the raw data.

Ethics approval and consent to participate

Not applicable.

Patient consent for publication

Not applicable.

Competing interests

The authors declare that they have no competing interests.

References

1. Lanctôt KL, Hviid Hahn-Pedersen J, Eichinger CS, Freeman C, Clark A, Tarazona LRS and Cummings J: Burden of illness in people with Alzheimer's disease: A systematic review of epidemiology, comorbidities and mortality. J Prev Alzheimers Dis 11: 97-107, 2024.
2. Heneka MT, van der Flier WM, Jessen F, Hoozemanns J, Thal DR, Boche D, Brosseron F, Teunissen C, Zetterberg H, Jacobs AH, *et al*: Neuroinflammation in Alzheimer disease. Nat Rev Immunol 25: 321-352, 2025.
3. Young-Pearse TL, Lee H, Hsieh YC, Chou V and Selkoe DJ: Moving beyond amyloid and tau to capture the biological heterogeneity of Alzheimer's disease. Trends Neurosci 46: 426-444, 2023.
4. Gao C, Jiang J, Tan Y and Chen S: Microglia in neurodegenerative diseases: Mechanism and potential therapeutic targets. Signal Transduct Target Ther 8: 359, 2023.
5. Orihuela R, McPherson CA and Harry GJ: Microglial M1/M2 polarization and metabolic states. Br J Pharmacol 173: 649-665, 2016.
6. Ward PS and Thompson CB: Metabolic reprogramming: A cancer hallmark even warburg did not anticipate. Cancer Cell 21: 297-308, 2012.
7. Zhang Y, Chen JC, Zheng JH, Cheng YZ, Weng WP, Zhong RL, Sun SL, Shi YS and Pan XD: Pterosin B improves cognitive dysfunction by promoting microglia M1/M2 polarization through inhibiting Klf5/Parp14 pathway. Phytomedicine 135: 156152, 2024.
8. Zhang D, Tang Z, Huang H, Zhou G, Cui C, Weng Y, Liu W, Kim S, Lee S, Perez-Neut M, *et al*: Metabolic regulation of gene expression by histone lactylation. Nature 574: 575-580, 2019.
9. Wang L, Cai Z, Gu Q and Xu C: cGAS deficiency regulates the phenotypic polarization and glycolysis of microglia through lactylation in hypoxic-ischemic encephalopathy cell model. Biochem Genet 62: 3961-3976, 2024.
10. Pan RY, He L, Zhang J, Liu X, Liao Y, Gao J, Liao Y, Yan Y, Li Q, Zhou X, *et al*: Positive feedback regulation of microglial glucose metabolism by histone H4 lysine 12 lactylation in Alzheimer's disease. Cell Metab 34: 634-648.e6, 2022.
11. Chang HC and Guarente L: SIRT1 and other sirtuins in metabolism. Trends Endocrinol Metab 25: 138-145, 2014.
12. Herskovits AZ and Guarente L: SIRT1 in neurodevelopment and brain senescence. Neuron 81: 471-483, 2014.
13. Rahman S and Islam R: Mammalian Sirt1: Insights on its biological functions. Cell Commun Signal 9: 11, 2011.
14. Lian B, Zhang J, Yin X, Wang J, Li L, Ju Q, Wang Y, Jiang Y, Liu X, Chen Y, *et al*: SIRT1 improves lactate homeostasis in the brain to alleviate parkinsonism via deacetylation and inhibition of PKM2. Cell Rep Med 5: 101684, 2024.
15. Tsukihara S, Akiyama Y, Shimada S, Hatano M, Igarashi Y, Taniai T, Tanji Y, Kodera K, Yasukawa K, Umeura K, *et al*: Delactylase effects of SIRT1 on a positive feedback loop involving the H19-glycolysis-histone lactylation in gastric cancer. Oncogene 44: 724-738, 2025.
16. Zhang N, Zhang Y, Xu J, Wang P, Wu B, Lu S, Lu X, You S, Huang X, Li M, *et al*: α-myosin heavy chain lactylation maintains sarcomeric structure and function and alleviates the development of heart failure. Cell Res 33: 679-698, 2023.
17. Li S, Lei Z and Sun T: The role of microRNAs in neurodegenerative diseases: A review. Cell Biol Toxicol 39: 53-83, 2023.
18. Jiao P, Wang XP, Luoreng ZM, Yang J, Jia L, Ma Y and Wei DW: miR-223: An effective regulator of immune cell differentiation and inflammation. Int J Biol Sci 17: 2308-2322, 2021.
19. La Rosa F, Mancuso R, Agostini S, Piancone F, Marventano I, Saresella M, Hernis A, Fenoglio C, Galimberti D, Scarpini E and Clerici M: Pharmacological and epigenetic regulators of NLRP3 inflammasome activation in Alzheimer's disease. Pharmaceuticals (Basel) 14: 1187, 2021.

20. Sánchez-Ceinos J, Rangel-Zuñiga OA, Clemente-Postigo M, Podadera-Herreros A, Camargo A, Alcalá-Diaz JF, Guzmán-Ruiz R, López-Miranda J and Malagón MM: miR-223-3p as a potential biomarker and player for adipose tissue dysfunction preceding type 2 diabetes onset. Mol Ther Nucleic Acids 23: 1035-1052, 2021.
21. Zhao Y, Zhong R, Deng C and Zhou Z: Circle RNA circABCB10 modulates PFN2 to promote breast cancer progression, as well as aggravate radioresistance through facilitating glycolytic metabolism Via miR-223-3p. Cancer Biother Radiopharm 36: 477-490, 2021.
22. Nunez-Iglesias J, Liu CC, Morgan TE, Finch CE and Zhou XJ: Joint genome-wide profiling of miRNA and mRNA expression in Alzheimer's disease cortex reveals altered miRNA regulation. PLoS One 5: e8898, 2010.
23. Lau P, Bossers K, Janky R, Salta E, Frigerio CS, Barbash S, Rothman R, Sierksma AS, Thathiah A, Greenberg D, *et al*: Alteration of the microRNA network during the progression of Alzheimer's disease. EMBO Mol Med 5::1613-1634, 2013.
24. Leidinger P, Backes C, Deutscher S, Schmitt K, Mueller SC, Frese K, Haas J, Ruprecht K, Paul F, Stähler C, *et al*: A blood based 12-miRNA signature of Alzheimer disease patients. Genome Biol 14: R78, 2013.
25. Wiedrick JT, Phillips JI, Lusardi TA, McFarland TJ, Lind B, Sandau US, Harrington CA, Lapidus JA, Galasko DR, Quinn JF and Saugstad JA: Validation of MicroRNA biomarkers for Alzheimer's disease in human cerebrospinal fluid. J Alzheimers Dis 67: 875-891, 2019.
26. Yu G, Wang LG, Han Y and He QY: clusterProfiler: An R package for comparing biological themes among gene clusters. OMICS 16: 284-287, 2012.
27. Liberzon A, Subramanian A, Pinchback R, Thorvaldsdóttir H, Tamayo P and Mesirov JP: Molecular signatures database (MSigDB) 3.0. Bioinformatics 27: 1739-1740, 2011.
28. Liberzon A, Birger C, Thorvaldsdóttir H, Ghandi M, Mesirov JP and Tamayo P: The molecular signatures database (MSigDB) hallmark gene set collection. Cell Syst 1: 417-425, 2015.
29. Duan JL, Ruan B, Song P, Fang ZQ, Yue ZS, Liu JJ, Dou GR, Han H and Wang L: Shear stress-induced cellular senescence blunts liver regeneration through Notch-sirtuin 1-P21/P16 axis. Hepatology 75: 584-599, 2022.
30. Kinney JW, Bemiller SM, Murtishaw AS, Leisgang AM, Salazar AM and Lamb BT: Inflammation as a central mechanism in Alzheimer's disease. Alzheimers Dement (N Y) 4: 575-590, 2018.
31. Kang YJ, Tan HY, Lee CY and Cho H: An air particulate pollutant induces neuroinflammation and neurodegeneration in human brain models. Adv Sci (Weinh) 8: e2101251, 2021.
32. McIntosh A, Mela V, Harty C, Minogue AM, Costello DA, Kerskens C and Lynch MA: Iron accumulation in microglia triggers a cascade of events that leads to altered metabolism and compromised function in APP/PS1 mice. Brain Pathol 29: 606-621, 2019.
33. Kong E, Li Y, Ma P, Zhang Y, Ding R, Hua T, Yang M and Yuan H: Lyn-mediated glycolysis enhancement of microglia contributes to neuropathic pain through facilitating IRF5 nuclear translocation in spinal dorsal horn. J Cell Mol Med 27: 1664-1681, 2023.
34. Baik SH, Kang S, Lee W, Choi H, Chung S, Kim JI and Mook-Jung I: A breakdown in metabolic reprogramming causes microglia dysfunction in Alzheimer's disease. Cell Metab 30: 493-507.e6, 2019.
35. Thapa R, Moglad E, Afzal M, Gupta G, Bhat AA, Hassan Almalki W, Kazmi I, Alzarea SI, Pant K, Singh TG, *et al*: The role of sirtuin 1 in ageing and neurodegenerative disease: A molecular perspective. Ageing Res Rev 102: 102545, 2024.
36. Razick DI, Akhtar M, Wen J, Alam M, Dean N, Karabala M, Ansari U, Ansari Z, Tabaie E and Siddiqui S: The role of sirtuin 1 (SIRT1) in neurodegeneration. Cureus 15: e40463, 2023.
37. Yang X, Zhou P, Zhao Z, Li J, Fan Z, Li X, Cui Z and Fu A: Improvement effect of mitotherapy on the cognitive ability of Alzheimer's disease through NAD^+/SIRT1-mediated autophagy. Antioxidants (Basel) 12: 2006, 2023.
38. Zhao W, Yang R, Meng X, Xu SQ, Li MM, Hao ZC, Wang SY, Jiang YK, Naseem A, Chen QS, *et al*: Panax quinquefolium saponins protects neuronal activity by promoting mitophagy in both in vitro and in vivo models of Alzheimer's disease. J Ethnopharmacol 340: 119250, 2025.
39. Li B, Chen Y, Zhou Y, Feng X, Gu G, Han S, Cheng N, Sun Y, Zhang Y, Cheng J, *et al*: Neural stem cell-derived exosomes promote mitochondrial biogenesis and restore abnormal protein distribution in a mouse model of Alzheimer's disease. Neural Regen Res 19: 1593-1601, 2024.
40. Cho SH, Chen JA, Sayed F, Ward ME, Gao F, Nguyen TA, Krabbe G, Sohn PD, Lo I, Minami S, *et al*: SIRT1 deficiency in microglia contributes to cognitive decline in aging and neurodegeneration via epigenetic regulation of IL-1β. J Neurosci 35: 807-818, 2015.
41. Wang J, Zhao R, Xu S, Zhou XY, Cai K, Chen YL, Zhou ZY, Sun X, Shi Y, Wang F, *et al*: NOTCH1 mitochondria localization during heart development promotes mitochondrial metabolism and the endothelial-to-mesenchymal transition in mice. Nat Commun 15: 9945, 2024.
42. Wang J, Zhu M, Zhu J, Li J, Zhu X, Wang K, Shen K, Yang K, Ni X, Liu X, *et al*: HES1 promotes aerobic glycolysis and cancer progression of colorectal cancer via IGF2BP2-mediated GLUT1 m6A modification. Cell Death Discov 9: 411, 2023.
43. Shi L, Liu S, Chen J, Wang H and Wang Z: Microglial polarization pathways and therapeutic drugs targeting activated microglia in traumatic brain injury. Neural Regen Res 21: 39-56, 2026.
44. Mo JS, Kim MY, Han SO, Kim IS, Ann EJ, Lee KS, Seo MS, Kim JY, Lee SC, Park JW, *et al*: Integrin-linked kinase controls Notch1 signaling by down-regulation of protein stability through Fbw7 ubiquitin ligase. Mol Cell Biol 27: 5565-5574, 2007.
45. Bellon M and Nicot C: Increased H19/miR-675 expression in adult T-cell leukemia is associated with a unique notch signature pathway. Int J Mol Sci 25: 5130, 2024.
46. Wu S, Wang Z, Zhu Y, Zhu X, Guo L, Fu Y, Zhang Q, Mou X and Liu Y: MiR-223-3p regulates the eosinophil degranulation and enhances the inflammation in allergic rhinitis by targeting FBXW7. Int Immunopharmacol 118: 110007, 2023.
47. Chen S, Lin J, Zhao J, Lin Q, Liu J, Wang Q, Mui R and Ma L: FBXW7 attenuates tumor drug resistance and enhances the efficacy of immunotherapy. Front Oncol 13: 1147239, 2023.